Mathematical and Computer Modelling 57 (2013) 2494–2509

Contents lists available at SciVerse ScienceDirect

Mathematical and Computer Modelling

journal homepage: www.elsevier.com/locate/mcm

Analytical solution for Hall and Ion-slip effects on mixed convection flow of couple stress fluid between parallel disks

D. Srinivasacharya *, K. Kaladhar

Department of Mathematics, National Institute of Technology, Warangal-506004, India

ARTICLE INFO

Article history:
Received 30 November 2011
Received in revised form 26 November 2012
Accepted 27 December 2012

Keywords:
Mixed convection
Couple stress fluid
MHD
Hall and Ion-slip effects
HAM

ABSTRACT

The Hall and Ion-slip effects on fully developed electrically conducting couple stress fluid flow between parallel disks has been considered. The governing non-linear partial differential equations are transformed into a system of ordinary differential equations using similarity transformations and then solved using Homotopy Analysis Method (HAM). The effects of the magnetic parameter, Hall parameter, Ion-Slip parameter, Prandtl number and couple stress fluid parameter on velocity and temperature are discussed and shown graphically.

1. Introduction

Rotating-disk flow has long been an important topic in fluid dynamic research for the interests in practical as well as academic senses. After the similarity analysis for the free-disk flow proposed by von Karman [1], numerous investigations have been carried out for the flow fields associated with either single-disk or two coaxial disks. Fluid flow and Heat transfer associated with a rotating disk system are of academic and practical interest for the wide applications of rotating machinery, lubrication, computer storage devices and crystal growth processes. Due to the massive applications of the heat transfer and also the rotating disk flows, it is important to establish some special theoretical results by which we can solve the Navier–Stokes equations. In the past decades, several researchers have explored the flow structure, heat and mass transfer characteristics associated with the rotating-disk flows. In a rapidly rotating system with the presence of the fluid temperature gradient, buoyancy effects induced by rotational forces may appear in the flow field. Under the Boussinesq approximation and invoking a density–temperature relation, a model for investigation of rotational buoyancy can be formulated. Soong [2] presented the theoretical analysis for axisymmetric mixed convection between rotating coaxial disks, later he studied the Prandtl number effects [3]. Dimian and Essawy [4] obtained the magnetic field effects on mixed convection between rotating coaxial disks. Soong [5] considered the non-isothermal flow mechanisms in rotating systems with emphasis on the rotation-induced thermal buoyancy effects stemming from the coexistence of rotational body forces and the non-uniformity of the fluid temperature field. Soong [6] studied the fluid flow and convective heat transfer between two co-axial disks rotating independently. Jiji and Ganatos [7] considered steady laminar flow and heat transfer generated by two infinite parallel disks. Atif and Tahir [8] investigated the effects of disks contracting, rotation and heat transfer on the viscous fluid between heated contracting rotating disks. Batista [9] obtained analytical solution of the Navier–Stokes equations for the case of the steady flow of an incompressible fluid between two uniformly co-rotating disks.

* Corresponding author. Tel.: +91 870 2462821; fax: +91 870 2459547.
E-mail addresses: dsrinivasacharya@yahoo.com, dsc@nitw.ac.in (D. Srinivasacharya).

0895-7177/$ – see front matter © 2012 Elsevier Ltd. All rights reserved.
doi:10.1016/j.mcm.2012.12.036

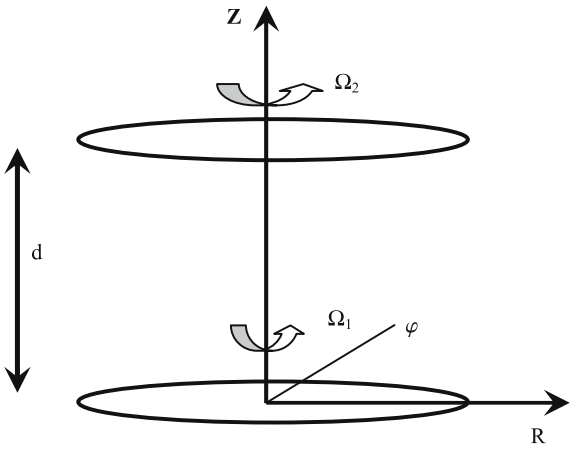

Fig. 1. Physical model and coordinate system.

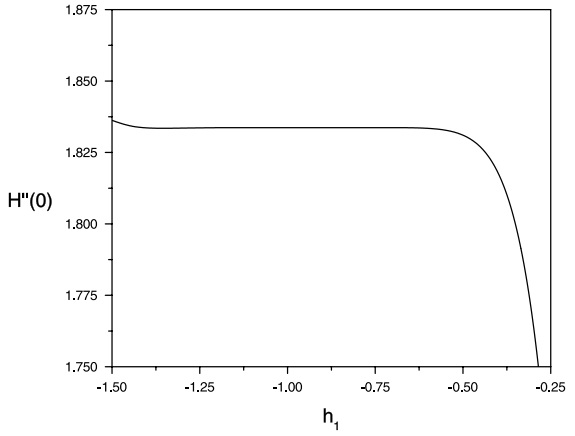

Fig. 2. h curve for $H(\eta)$.

The mixed convection flow of an electrically conducting fluid between rotating disks in the presence of an axial magnetic field is of special technical significance because of its frequent occurrence in many industrial applications such as petroleum technology to study the movement of natural gas, oil and water through the oil reservoirs, in chemical engineering for filtration and purification process, in agriculture engineering to study the underground water resources etc. This type of problem also arises in electronic packages, microelectronic devices during their operations. In recent years, several investigators have extended many of the available convection heat transfer and fluid flow problems to include the effects of magnetic fields for those cases when the fluid is electrically conducting. Ibrahim [10] considered the unsteady flow between two rotating disks with heat transfer. The magnetohydrodynamic effects on a fluid film squeezed between two rotating surfaces presented by Hamza [11]. Kumari et al. [12] discussed the unsteady flow of a viscous fluid between two parallel disks with a time varying gap width and a magnetic field. In most of the MHD flow problems, the Hall and Ion-slip terms in Ohm's law were ignored. However, in the presence of strong magnetic field, the influence of Hall current and Ion-slip are important. Attia [13] considered the flow due to a rotating disk, taking the Ion-slip into consideration. Hall and Ion-Slip effects on three-dimensional flow of a second grade fluid presented by Hayat and Nawaz [14].

The classical Navier–Stokes theory does not describe the flow properties of polymeric fluids, colloidal suspension and fluids containing certain additives. Different models have been proposed to explain the behavior of such fluids. Stokes [15] proposed the theory of couple stress fluids, which shows the size dependent effect in the presence of couple stresses, body couples and non-symmetric stress tensor. These fluids are capable of describing various types of lubricants, blood, suspension fluids etc. The study of couple-stress fluids has applications in a number of processes that occur in industry such as the extrusion of polymer fluids, solidification of liquid crystals, cooling of metallic plate in a bath, and colloidal solutions etc. Stokes [15] discussed the hydro-magnetic steady flow of a fluid with couple stress effects. A review of couple stress (polar) fluid dynamics was reported by Stokes [16]. Also, the study of magnetohydrodynamics and couple stress fluid with Hall and ion-slip currents with heat transfer has important engineering application e.g. in power generators, MHD accelerators, refrigeration coils, transmission lines, electric transformers and heating elements. Recently, Srinivasacharya and Kaladhar [17,18] discussed the convection flow of couple stress fluid in vertical channel with Hall and Ion-slip effects.

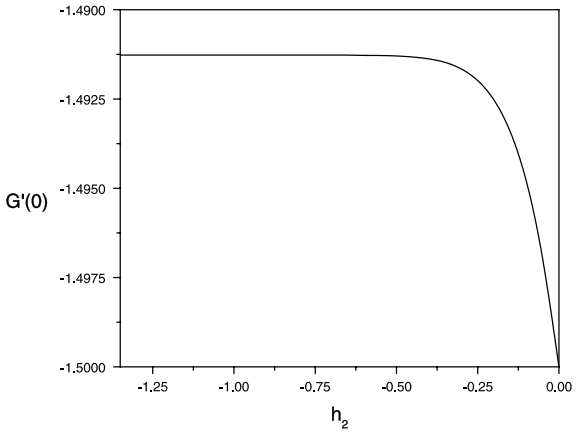

Fig. 3. h curve for $G(\eta)$.

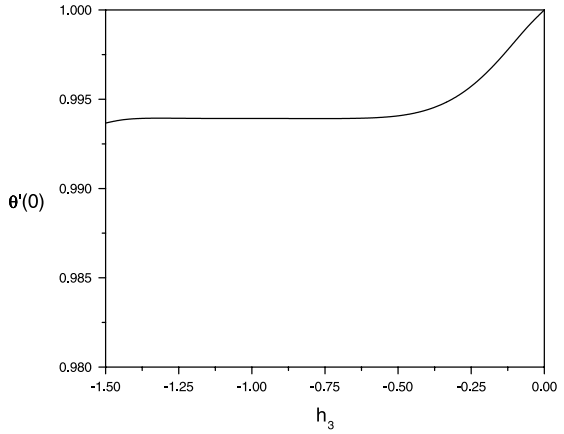

Fig. 4. h curve for $\theta(\eta)$.

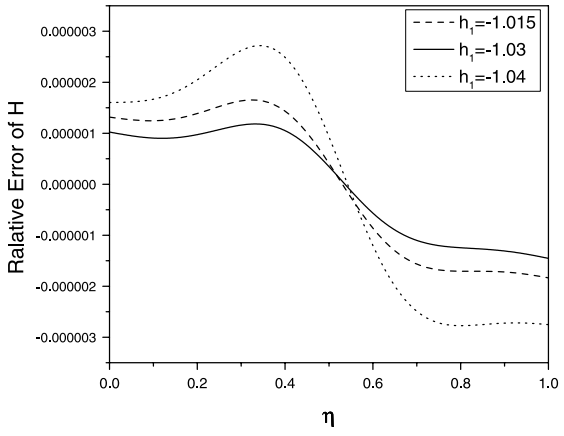

Fig. 5. Relative error of $H(\eta)$.

In the present work the mixed convection in couple stress fluid with heat transfer flow between two infinite rotating disks in an axial uniform steady magnetic field is studied, considering both the Hall effect and the Ion-Slip. The Homotopy Analysis method is employed to solve the governing nonlinear equations. The homotopy analysis method was first proposed by Liao [19] in 1992, is one of the most efficient methods in solving different types of nonlinear equations such as coupled, decoupled, homogeneous and non-homogeneous. Also, HAM provides us a great freedom to choose different base functions to express solutions of a nonlinear problem [20]. Convergence of the derived series solution is analyzed. The behavior of emerging flow parameters on the velocity and temperature is discussed.

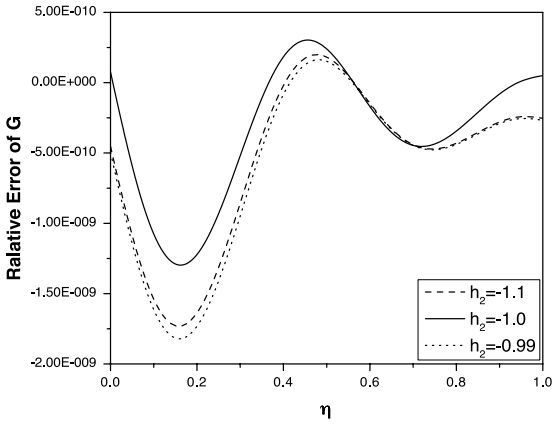

Fig. 6. Relative error of $G(\eta)$.

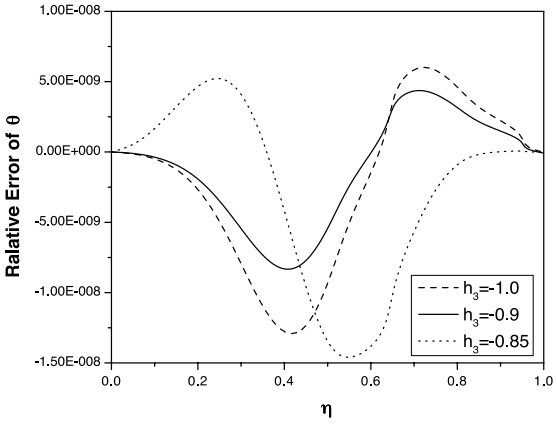

Fig. 7. Relative error of $\theta(\eta)$.

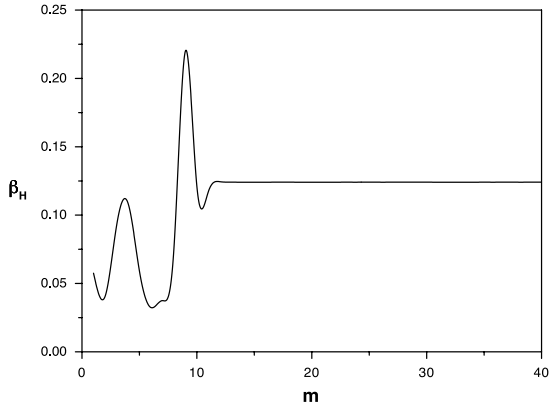

Fig. 8. The ratio β_H from the theorem to reveal the convergence of the HAM solutions.

2. Mathematical formulation

Consider the axisymmetric steady flow of a incompressible couple stress fluid with Hall and Ion-Slip effects between two horizontal parallel infinite disks separated by a spacing d. The disks lie at constant temperatures T_1 and T_2, and rotate with rotational speeds Ω_1 and Ω_2, respectively, as shown in Fig. 1. Cylindrical coordinates (R, φ, Z) are fixed on the lower disk and their origin lies at the disk center. It is assumed that the gravitational force and the stress work effects are negligibly small. The flow is assumed laminar with constant properties. The Coriolis force $(2\rho\overline{\Omega} \times \overline{q})$ and centrifugal forces $(\rho\overline{\Omega} \times (\overline{\Omega} \times \overline{R})$, where $\overline{R}$ is the position vector) due to disk-rotation appear in momentum balance explicitly and, therefore, Boussinesq

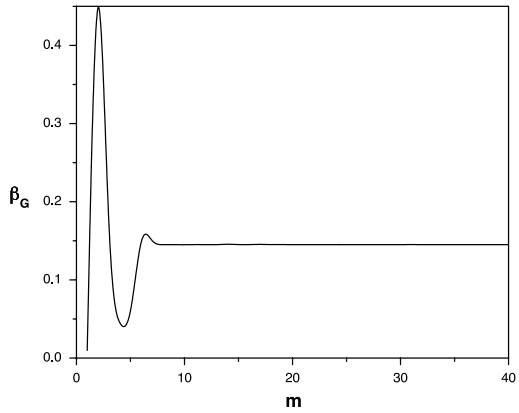

Fig. 9. The ratio β_G from the theorem to reveal the convergence of the HAM solutions.

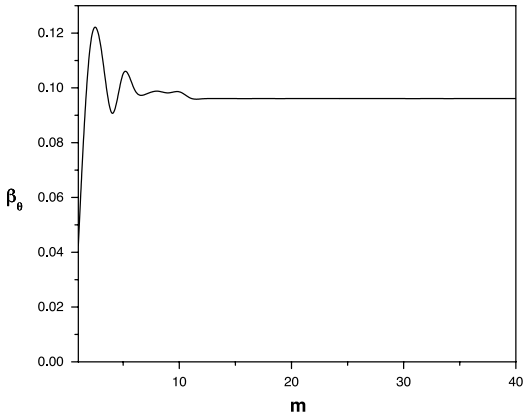

Fig. 10. The ratio β_θ from the theorem to reveal the convergence of the HAM solutions.

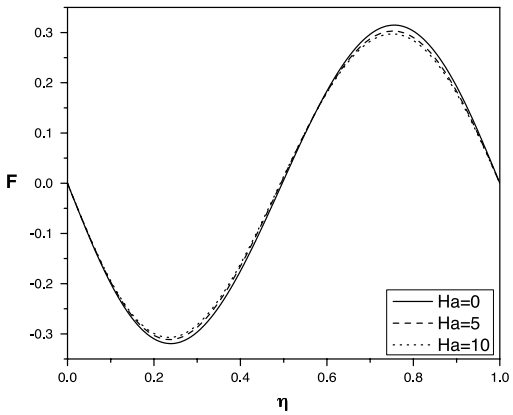

Fig. 11. Magnetic effect (Ha) on F at $\gamma = -1$, $Re = 50$, $\beta_h = 0.20$, $\beta_i = 0.20$, $Pr = 0.01$, $S = 1.0$.

approximation can be easily implemented i.e. the density associated with the terms of gravity, the centrifugal and the Coriolis forces due to the disk rotation, and the curvilinear motion of the fluids are all considered as variable. The linear density–temperature relation, $\rho = \rho_r[1 - \beta(T - T_r)]$, is employed for accounting the rotational buoyancy effects induced by the body forces [5,6]. The subscript r denotes the reference condition and the parameter β is the thermal-expansion coefficient. In the present study, the wall condition of disk 1 is used as the reference state. The reference state is of conditions $\overline{q} = 0$, $T = T_r$, $\rho = \rho_r$ and $P = P_r$. At the reference state, the original momentum equation can be reduced to $\nabla P_r/\rho_r = \overline{\Omega} \times (\overline{\Omega} \times \overline{R}) + \overline{g}$, which is the conservative part of the centrifugal and gravitational forces in flow field. A magnetic field of strength B_0 is applied normal to the disk surface, and it is assumed that the magnetic Reynolds number is small. Hence the induced magnetic field can be neglected, as compared to the applied magnetic field. Further, the electron-atom

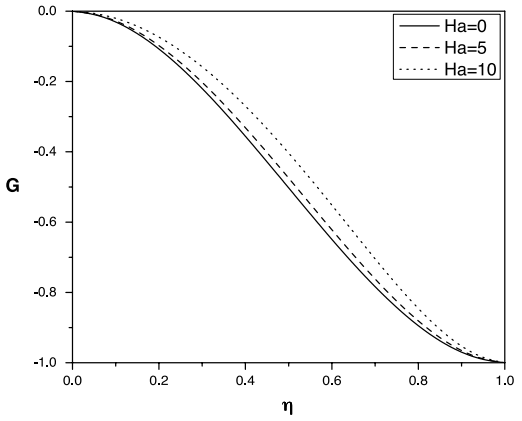

Fig. 12. Magnetic effect (Ha) on G at $\gamma = -1$, $Re = 50$, $\beta_h = 0.20$, $\beta_i = 0.20$, $Pr = 0.01$, $S = 1.0$.

collision frequency is assumed to be relatively high, so that the Hall effect and the ion slip cannot be neglected. With the above considerations and approximations, the governing equations for the flow can be depicted [15,5], as

$$\nabla \cdot \overline{q} = 0, \tag{1}$$

$$(\overline{q} \cdot \nabla)\overline{q} + 2[1 - \beta(T - T_r)](\overline{\Omega} \times \overline{q}) + \beta(T - T_r)\overline{\Omega} \times (\overline{\Omega} \times \overline{R}) - \beta(T - T_r)\overline{g} = \frac{-\nabla P*}{\rho_r}$$

$$- \nu\nabla \times \nabla \times \overline{q} - \frac{\eta_1}{\rho_r}\nabla \times \nabla \times \nabla \times \nabla \times \overline{q} + \frac{\overline{J} \times \overline{B}}{\rho_r} \tag{2}$$

$$(\overline{q} \cdot \nabla)T = \alpha\nabla^2 T \tag{3}$$

in which $P^* = P - P_r$ is the pressure departure from the reference condition, $\overline{\Omega} = \Omega_1\overline{e_z}$, $\overline{R} = R\overline{e_r}$, $\overline{e_z}$ and $\overline{e_r}$ are the unit vectors in the axial and radial directions, respectively. The last two terms on Left hand side of Eq. (2) are vorticity generation by centrifugal buoyancy and Coriolis effect, respectively. Let the velocity components in the R, φ and Z directions are U, V and W, respectively. In the present analysis, the following dimensionless variables are used,

$$U = R\Omega_1 F(\eta), \qquad V = R\Omega_1 G(\eta), \qquad W = \sqrt{\nu\Omega_1}H(\eta), \quad \eta = \frac{Z}{d}, \qquad T - T_1 = \Delta T\theta$$

where $\Delta T = T_2 - T_1$ is the characteristic temperature difference. G, H, and θ are the tangential, axial velocities and the temperature function, respectively. The transformation is essentially of von Karman type but with an additional treatment to the temperature function in the energy equation. The governing equations (1)–(3) can thus be cast into the following dimensionless form:

$$S^2H^{vi} - H^{iv} + 4Re^{3/2}[(1 + G)G' - B(G\theta' + G'\theta)] + Re^{1/2}HH''' - 2BRe^{3/2}\theta'$$
$$+ \frac{Ha^2\alpha_e H''}{\alpha_e^2 + \beta_h^2} + 2\frac{Re^{1/2}Ha^2\beta_h}{\alpha_e^2 + \beta_h^2}G' = 0 \tag{4}$$

$$S^2G^{iv} + Re^{1/2}[HG' - H'G - H' + BH'\theta] - G'' - \frac{1}{2}\frac{Ha^2Re^{1/2}\beta_h H'}{\alpha_e^2 + \beta_h^2} + \frac{Ha^2\alpha_e}{\alpha_e^2 + \beta_h^2}G = 0 \tag{5}$$

$$\theta'' = PrRe^{1/2}H\theta' \tag{6}$$

in which the continuity equation

$$H' = 2Re^{1/2}F \tag{7}$$

has been introduced to simplify the system by eliminating the radial velocity function $F(\eta)$. The superscript $()'$ denotes differentiation with respect to η, Eqs. (4) and (5), respectively, are the radial and circumferential components of the momentum equation (2). Here $Pr = \frac{\nu}{\alpha}$ is the Prandtl number which indicates the relative importance of viscous to thermal diffusion effects, $Re = \frac{d^2\Omega_1}{\nu}$ is the Reynolds number which characterizes the rotational effect, its range is from 50 to 500, $B = \beta\Delta T$ is the thermal Rossby number which measures the buoyancy effect, β_h, β_i indicates the Hall and Ion-slip effects. $Ha = B_0 d\sqrt{\frac{\sigma}{\mu}}$ is the Hartmann number implies the Magnetic effect, $S = \frac{1}{d}\sqrt{\frac{\eta_1}{\mu}}$ is the Couple stress parameter. The effects of couple-stress are significant for large values of $S(= l/d)$, where $l = \sqrt{\frac{\eta_1}{\mu}}$ is the material constant. If l is a function of the

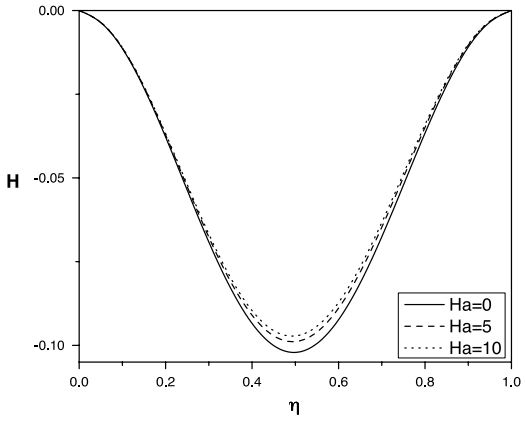

Fig. 13. Magnetic effect (Ha) on H at $\gamma = -1$, $Re = 50$, $\beta_h = 0.20$, $\beta_i = 0.20$, $Pr = 0.01$, $S = 1.0$.

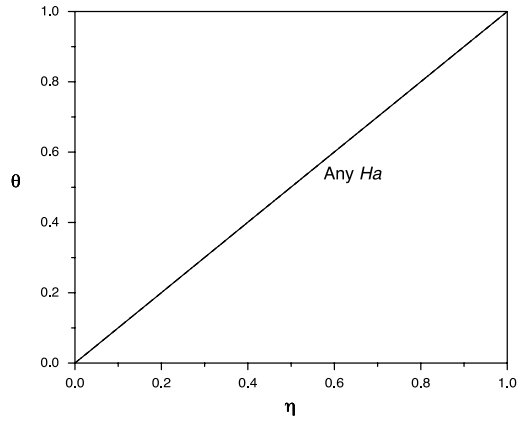

Fig. 14. Magnetic effect (Ha) on θ at $\gamma = -1$, $Re = 50$, $\beta_h = 0.20$, $\beta_i = 0.20$, $Pr = 0.01$, $S = 1.0$.

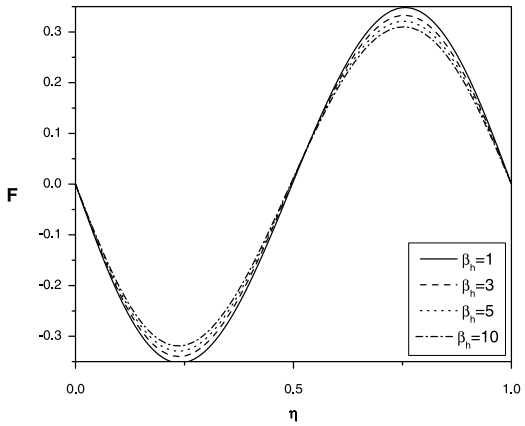

Fig. 15. Effect of β_h on F at $\gamma = -1$, $Re = 50$, $Pr = 0.01$, $\beta_i = 0.20$, $S = 1.0$, $Ha = 10.0$.

molecular dimensions of the liquid, it will vary greatly for different liquids. For example, the length of a polymer chain may be a million times the diameter of water molecule [15]. Therefore, there are all the reasons to expect that couple-stresses appear in noticeable magnitudes in liquids with large molecules.

The parameter $\gamma = \frac{\Omega_2 - \Omega_1}{\Omega_1}$ denotes the relative rotation rate of the disk 2 with respect to that of the disk 1. For example, the values of $\gamma = 0$ and $\gamma = -1$ correspond to the cases of co-rotating disks ($\Omega_1 = \Omega_2$) and rotor–stator ($\Omega_1 \neq \Omega_2$), respectively. Note that, in this two-disk flow configuration, the cases of $\gamma = 0$ and $B \neq 0$ are the pure free-convection. While the forced convection is characterized by $\gamma \neq 0$ and $B = 0$. For the non-zero B as well as γ, the problem becomes a mixed convection one, in which Re can be used to characterize the forced flow effect.

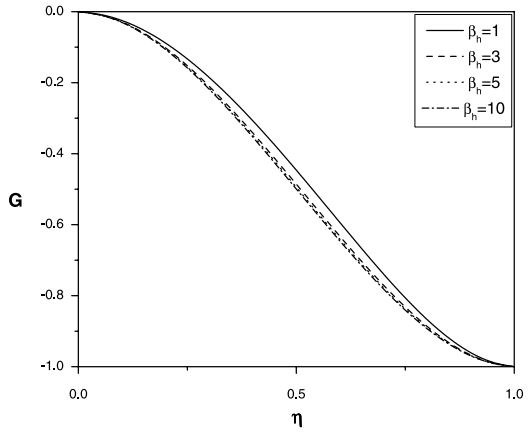

Fig. 16. Effect of β_h on G at $\gamma = -1$, $Re = 50$, $Pr = 0.01$, $\beta_i = 0.20$, $S = 1.0$, $Ha = 10.0$.

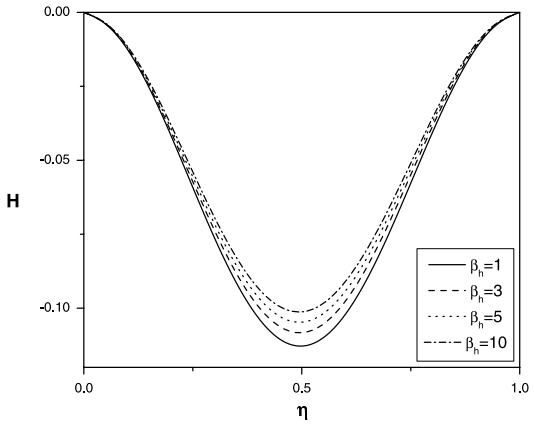

Fig. 17. Effect of β_h on H at $\gamma = -1$, $Re = 50$, $Pr = 0.01$, $\beta_i = 0.20$, $S = 1.0$, $Ha = 10.0$.

Boundary conditions

On the disks, according to the no-slip condition, the radial and axial velocities are zero. The tangential velocity G at the disk l is identically zero; however, due to relative motion of two disks, the tangential velocity at disk 2 is $R(\Omega_2 - \Omega_1)$. Thermal boundary conditions at disk 1 and disk 2 are uniform wall temperatures T_1 and T_2, respectively. By defining a dimensionless rotation rate for disk 2, the boundary conditions can be written as

.

$$H(0) = 0, \quad H'(0) = 0, \quad G(0) = 0, \quad H(1) = 0, \quad H'(1) = 0, \quad G(1) - \gamma = 0, \quad \theta(0) = 0, \quad \theta(1) = 1 \tag{8a}$$

$$H'''(0) = 0, \quad H'''(1) = 0, \quad G'(0) = 0, \quad G'(1) = 0. \tag{8b}$$

The boundary condition (8b) imply that the couple stresses are zero at the disk surfaces.

3. The HAM solution of the problem

For HAM solutions, we choose the initial approximations of $H(\eta)$, $G(\eta)$ and $\theta(\eta)$ as follows:

$$H_0(\eta) = 0, \quad G_0(\eta) = \gamma(3\eta^2 - 2\eta^3), \quad \theta_0(\eta) = \eta; \tag{9}$$

and choose the auxiliary linear operators:

$$L_1 = \frac{\partial^6}{\partial \eta^6}, \quad L_2 = \frac{\partial^4}{\partial \eta^4}, \quad L_3 = \frac{\partial^2}{\partial \eta^2} \tag{10}$$

such that

$$L_1(c_1 + c_2\eta + c_3\eta^2 + c_4\eta^3 + c_5\eta^4 + c_6\eta^5) = 0, \quad L_2(c_7 + c_8\eta + c_9\eta^2 + c_{10}\eta^3) = 0 \quad L_3(c_{11} + c_{12}\eta) = 0 \tag{11}$$

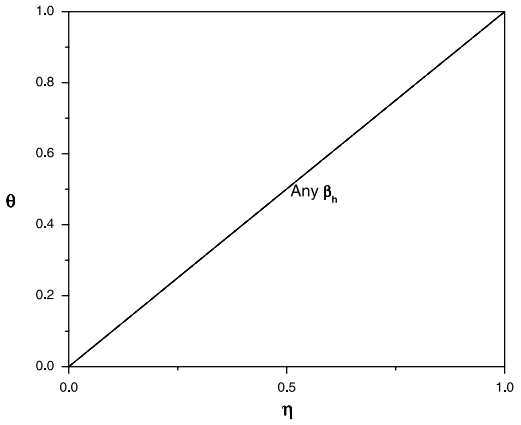

Fig. 18. Effect of β_h on θ at $\gamma = -1$, $Re = 50$, $Pr = 0.01$, $\beta_i = 0.20$, $S = 1.0$, $Ha = 10.0$.

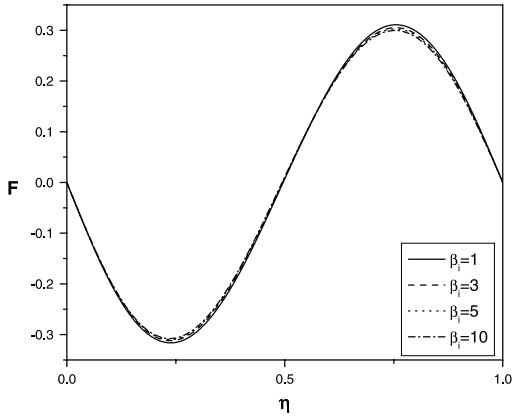

Fig. 19. Effect of β_i on F at $\gamma = -1$, $Re = 50$, $Pr = 0.01$, $\beta_h = 0.20$, $S = 1.0$, $Ha = 10.0$.

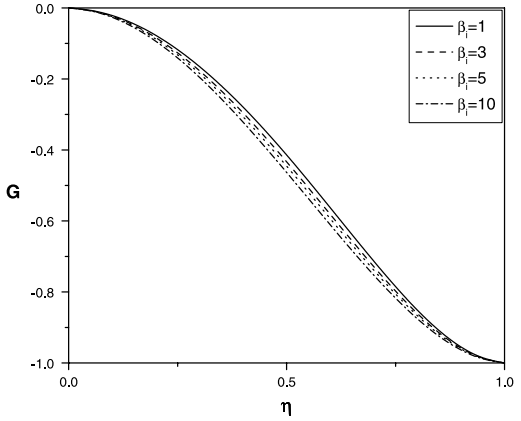

Fig. 20. Effect of β_i on G at $\gamma = -1$, $Re = 50$, $Pr = 0.01$, $\beta_h = 0.20$, $S = 1.0$, $Ha = 10.0$.

where c_i ($i = 1, 2, \ldots, 12$) are constants. Introducing non-zero auxiliary parameters h_1, h_2 and h_3, we develop the zeroth-order deformation problems as follow:

$$(1 - p)L_1[H(\eta; p) - H_0(\eta)] = ph_1N_1[H(\eta; p)] \tag{12}$$

$$(1 - p)L_2[G(\eta; p) - G_0(\eta)] = ph_2N_2[G(\eta; p)] \tag{13}$$

$$(1 - p)L_3[\theta(\eta; p) - \theta_0(\eta)] = ph_3N_3[\theta(\eta; p)] \tag{14}$$

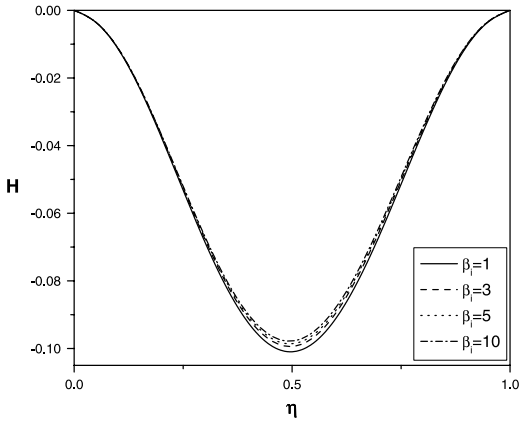

Fig. 21. Effect of β_i on H at $\gamma = -1$, $Re = 50$, $Pr = 0.01$, $\beta_h = 0.20$, $S = 1.0$, $Ha = 10.0$.

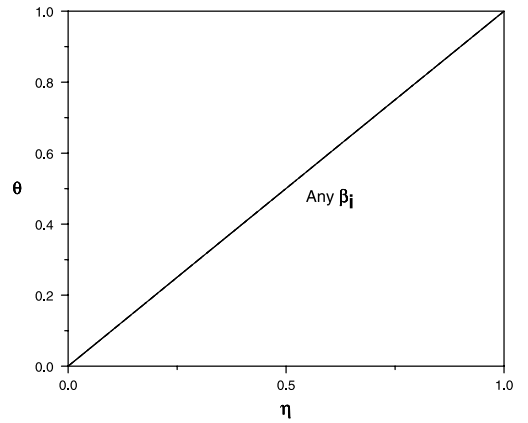

Fig. 22. Effect of β_i on θ at $\gamma = -1$, $Re = 50$, $Pr = 0.01$, $\beta_h = 0.20$, $S = 1.0$, $Ha = 10.0$.

subject to the boundary conditions

$$\begin{aligned} &H(0;p) = 0, \quad H'(0;p) = 0, \quad G(0;p) = 0, \quad H'''(0;p) = 0, \quad G'(0;p) = 0 \\ &H(1;p) = 0, \quad H'(1;p) = 0, \quad G(1;p) = \gamma, \quad H'''(1;p) = 0 \quad G'(1;p) = 0 \\ &\theta(0;p) = 0, \quad \theta(1;p) = 1 \end{aligned} \tag{15}$$

where $p \in [0, 1]$ is the embedding parameter and the non-linear operators N_1, N_2 and N_3 are defined as:

$$\begin{aligned} N_1[H(\eta,p), G(\eta,p), \theta(\eta,p)] \;=\; & S^2 H^{vi} - H^{iv} + 4Re^{3/2}[(1+G)G' - B(G\theta' + G'\theta)] \\ & + Re^{1/2} HH''' - 2BRe^{3/2}\theta' + \frac{Ha^2\alpha_e}{\alpha_e^2+\beta_h^2}H'' + 2\frac{Re^{1/2}Ha^2\beta_h}{\alpha_e^2+\beta_h^2}G' \end{aligned} \tag{16}$$

$$\begin{aligned} N_2[H(\eta,p), G(\eta,p), \theta(\eta,p)] \;=\; & S^2 G^{iv} + Re^{1/2}[HG' - H'G - H' + BH'\theta] - G'' \\ & - \frac{1}{2}\frac{Ha^2 Re^{1/2}\beta_h}{\alpha_e^2+\beta_h^2}H' + \frac{Ha^2\alpha_e}{\alpha_e^2+\beta_h^2}G \end{aligned} \tag{17}$$

$$N_3[H(\eta,p), G(\eta,p), \theta(\eta,p)] = \theta'' - PrRe^{1/2}H\theta'. \tag{18}$$

For $p = 0$, we have the initial guess approximations

$$H(\eta;0) = H_0(\eta), \quad G(\eta;0) = G_0(\eta), \quad \theta(\eta;0) = \theta_0(\eta). \tag{19}$$

When $p = 1$, Eqs. (12)–(14) are same as (4)–(6) respectively, therefore at $p = 1$ we get the final solutions

$$H(\eta;1) = H(\eta), \quad G(\eta;1) = G(\eta) \quad \theta(\eta;1) = \theta(\eta). \tag{20}$$

Hence the process of giving an increment to p from 0 to 1 is the process of $H(\eta; p)$ varying continuously from the initial guess $H_0(\eta)$ to the final solution $H(\eta)$ (similar for $G(\eta, p)$ and $\theta(\eta, p)$). This kind of continuous variation is called deformation in

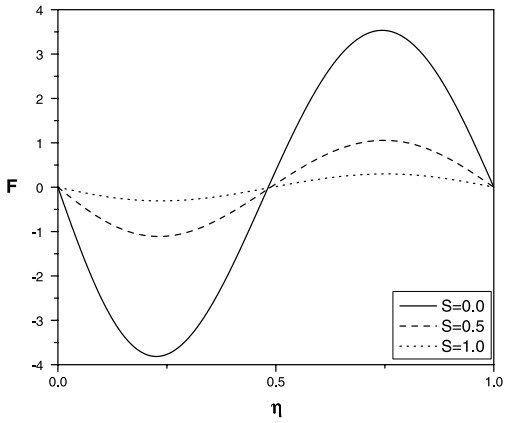

Fig. 23. Effect of S on F at $\gamma = -1$, $Re = 50$, $Pr = 0.01$, $\beta_i = 2.0$, $\beta_h = 2.0$, $Ha = 5.0$.

topology so that we call system Eqs. (12)–(15), the zeroth-order deformation equation. Next, the mth-order deformation equations follow as

$$L_1[H_m(\eta) - \chi_m H_{m-1}(\eta)] = h_1 R_m^H(\eta), \tag{21}$$

$$L_2[G_m(\eta) - \chi_m G_{m-1}(\eta)] = h_2 R_m^G(\eta), \tag{22}$$

$$L_3[\theta_m(\eta) - \chi_m \theta_{m-1}(\eta)] = h_3 R_m^\theta(\eta), \tag{23}$$

with the boundary conditions

$$\begin{aligned} &H_m(0) = 0, \quad H_m'(0) = 0, \quad G_m(0) = 0, \quad H_m'''(0) = 0, \quad G_m'(0) = 0 \\ &H_m(1) = 0, \quad H_m'(1) = 0, \quad G_m(1) = 0, \quad H_m'''(1) = 0 \quad G_m'(1) = 0 \\ &\theta_m(0) = 0, \quad \theta_m(1) = 0 \end{aligned} \tag{24}$$

where

$$\begin{aligned} R_m^H(\eta) \;=\; & S^2 H^{vi} - H^{iv} + 4Re^{3/2}\left[G' + \sum_{n=0}^{m-1} G'_{m-1-n} G_n - B\sum_{n=0}^{m-1}(G_n \theta'_{m-1-n} + G'_{m-1-n}\theta_n)\right] \\ & + Re^{1/2}\sum_{n=0}^{m-1} H_n H'''_{m-1-n} - 2BRe^{3/2}\theta' + \frac{Ha^2\alpha_e}{\alpha_e^2+\beta_h^2}H'' + 2\frac{Re^{1/2}Ha^2\beta_h}{\alpha_e^2+\beta_h^2}G' \end{aligned} \tag{25}$$

$$\begin{aligned} R_m^G(\eta) \;=\; & S^2 G^{iv} + Re^{1/2}\left[\sum_{n=0}^{m-1}(H_n G'_{m-1-n} - H'_{m-1-n}G_n + BH'_{m-1-n}\theta_n) - H'\right] - G'' \\ & - \frac{1}{2}\frac{Ha^2 Re^{1/2}\beta_h}{\alpha_e^2+\beta_h^2}H' + \frac{Ha^2\alpha_e}{\alpha_e^2+\beta_h^2}G \end{aligned} \tag{26}$$

$$R_m^\theta(\eta) = \theta'' = PrRe^{1/2}\sum_{n=0}^{m-1} H_n \theta'_{m-1-n} \tag{27}$$

and, for m being integer

$$\begin{aligned} \chi_m \;&=\; 0 \quad \text{for } m \le 1 \\ &=\; 1 \quad \text{for } m > 1. \end{aligned} \tag{28}$$

The initial guess approximations $H_0(\eta)$, $G_0(\eta)$ and $\theta_0(\eta)$, the linear operators L_1, L_2 and L_3 and the auxiliary parameters h_1, h_2 and h_3 are assumed to be selected such that equations (12)–(15) have solution at each point $p \in [0, 1]$ and also with the help of Taylor series and due to Eq. (19) $H(\eta; p)$, $G(\eta; p)$ and $\theta(\eta; p)$ can be expressed as

$$H(\eta; p) = H_0(\eta) + \sum_{m=1}^{\infty} H_m(\eta) p^m \tag{29}$$

$$G(\eta; p) = G_0(\eta) + \sum_{m=1}^{\infty} G_m(\eta) p^m \tag{30}$$

$$\theta(\eta; p) = \theta_0(\eta) + \sum_{m=1}^{\infty} \theta_m(\eta) p^m \tag{31}$$

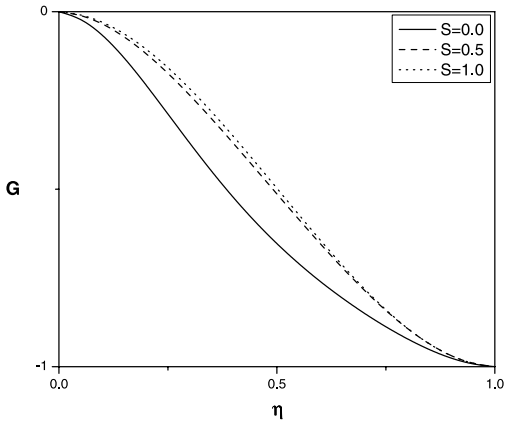

Fig. 24. Effect of S on G at $\gamma = -1$, $Re = 50$, $Pr = 0.01$, $\beta_i = 2.0$, $\beta_h = 2.0$, $Ha = 5.0$.

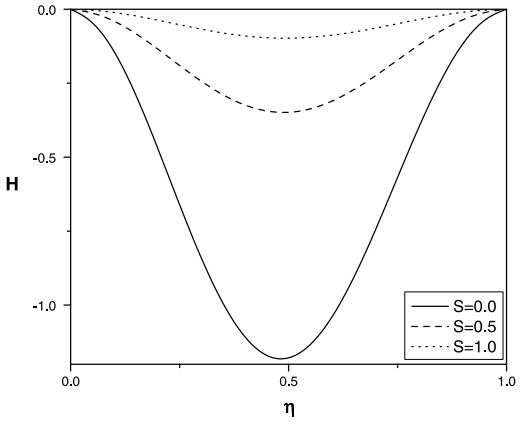

Fig. 25. Effect of S on H at $\gamma = -1$, $Re = 50$, $Pr = 0.01$, $\beta_i = 2.0$, $\beta_h = 2.0$, $Ha = 5.0$.

in which h_1, h_2 and h_3 are chosen in such a way that the series (29)–(31) are convergent at $p = 1$. Therefore we have from (20) that

$$H(\eta) = H_0(\eta) + \sum_{m=1}^{\infty} H_m(\eta), \tag{32}$$

$$G(\eta) = G_0(\eta) + \sum_{m=1}^{\infty} G_m(\eta) \tag{33}$$

$$\theta(\eta) = \theta_0(\eta) + \sum_{m=1}^{\infty} \theta_m(\eta) \tag{34}$$

for which we presume that the initial guesses to H, G and θ the auxiliary linear operators L and the non-zero auxiliary parameters h_1, h_2 and h_3 are so properly selected that the deformation $H(\eta, p)$, $G(\eta, p)$ and $\theta(\eta, p)$ are smooth enough and their mth-order derivatives with respect to p in equations (32)–(34) exist and are given respectively by $H_m(\eta) = \frac{1}{m!}\frac{\partial^m H(\eta;p)}{\partial p^m}\Big|_{p=0}$, $G_m(\eta) = \frac{1}{m!}\frac{\partial^m G(\eta;p)}{\partial p^m}\Big|_{p=0}$, $\theta_m(\eta) = \frac{1}{m!}\frac{\partial^m \theta(\eta;p)}{\partial p^m}\Big|_{p=0}$. It is clear that the convergence of Taylor series at $p = 1$ is a prior assumption, whose justification is provided via a theorem [21], so that the system in (32)–(34) holds true. The formulas in (32)–(34) provide us with a direct relationship between the initial guesses and the exact solutions. All the effects of interaction of the magnetic field as well as of the heat transfer, Hall and Ion effects and couple stress flow field can be studied from the exact formulas (32)–(34). Moreover, a special emphasize should be placed here that the mth-order deformation system (21)–(24) is a linear differential equation system with the auxiliary linear operators L whose fundamental solution is known.

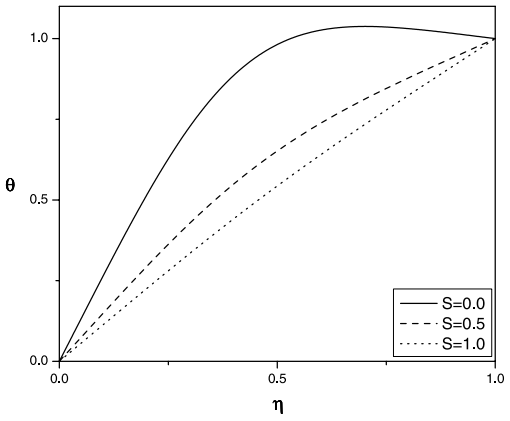

Fig. 26. Effect of S on θ at $\gamma = -1$, $Re = 50$, $Pr = 0.01$, $\beta_i = 2.0$, $\beta_h = 2.0$, $Ha = 5.0$.

4. Convergence of the HAM solution

The expressions for H, G and θ contain the auxiliary parameters h_1, h_2 and h_3. As pointed out by Liao [19], the convergence and the rate of approximation for the HAM solution strongly depend on the values of auxiliary parameter h. For this purpose, h-curves are plotted by choosing h_1, h_2 and h_3 in such a manner that the solutions (29)–(31) ensure convergence [19]. Here to see the admissible values of h_1, h_2 and h_3, the h-curves are plotted for 15th-order of approximation in Figs. 2–4 by taking the values of the parameters $Re = 50$, $Ha = 2.0$, $\beta_h = 2.0$, $\beta_i = 2.0$, $Pr = 0.01$, $S = 1$, $\gamma = -1$, and $B = 0.05$. It is clearly noted from Fig. 2 that the range for the admissible values of h_1 is $-1.35 < h_1 < -0.6$. From Fig. 3, it can be seen that the h-curve has a parallel line segment that corresponds to a region $-1.5 < h_2 < -0.6$. Fig. 4 depicts that the admissible value of h_3 are $-1.25 < h_3 < -0.6$. A wide valid zone is evident in these figures ensuring convergence of the series. To choose optimal value of auxiliary parameter, the average residual errors (see Ref. [22] for more details) are defined as

$$E_{H,m} = \frac{1}{K}\sum_{i=0}^{K}\left(N_1\left[\sum_{j=0}^{m} H_j(i\Delta t)\right]\right)^2 \tag{35}$$

$$E_{G,m} = \frac{1}{K}\sum_{i=0}^{K}\left(N_2\left[\sum_{j=0}^{m} G_j(i\Delta t)\right]\right)^2 \tag{36}$$

$$E_{\theta,m} = \frac{1}{K}\sum_{i=0}^{K}\left(N_3\left[\sum_{j=0}^{m} \theta_j(i\Delta t)\right]\right)^2 \tag{37}$$

where $\Delta t = 1/K$ and $K = 5$. At different order of approximations (m), minimum of average residual errors are shown in Tables 1–3. It is clear from Table 1 that the average residual error for H is minimum at $h_1 = -1.03$. It can be seen from Table 2 that the minimum of average residual error for W attains at $h_2 = -1$. Table 3 depicts that at $h_3 = -0.9$, E_θ attains minimum. Therefore, the optimum values of convergence control parameters are taken as $h_1 = -1.03,\ h_2 = -1,\ h_3 = -0.9$.

To see the accuracy of the solutions, the residual errors are defined for the system as

$$\begin{aligned} RE_H &= S^2 H_n^{vi} - H_n^{iv} + 4Re^{3/2}[(1+G_n)G_n' - B(G_n\theta_n' + G_n'\theta_n)] + Re^{1/2}H_nH_n''' - 2BRe^{3/2}\theta_n' \\ &\quad + \frac{Ha^2\alpha_e}{\alpha_e^2+\beta_h^2}H_n'' + 2\frac{Re^{1/2}Ha^2\beta_h}{\alpha_e^2+\beta_h^2}G_n' \end{aligned} \tag{38}$$

$$RE_G = S^2 G_n^{iv} + Re^{1/2}[H_nG_n' - H_n'G_n - H_n' + BH_n'\theta_n] - G_n'' - \frac{1}{2}\frac{Ha^2Re^{1/2}\beta_h}{\alpha_e^2+\beta_h^2}H_n' + \frac{Ha^2\alpha_e}{\alpha_e^2+\beta_h^2}G_n \tag{39}$$

$$RE_\theta = \theta'' = PrRe^{1/2}H\theta' \tag{40}$$

where $H_n(\eta)$, $G_n(\eta)$ and $\theta_n(\eta)$ are the HAM solution for $H(\eta)$, $G(\eta)$ and $\theta(\eta)$. For optimality of the convergence control parameters, residual error for different values of h in the convergence region displayed in Figs. 5–7. We examine that $h_1 = -1.03,\ h_2 = -1,\ h_3 = -0.9$ gives a better solution. Table 4 establishes the convergence of the obtained series solution. It is found from the above observations that the series given by (29)–(31) converge in the whole region of η when $h_1 = -1.03$, $h_2 = -1,\ h_3 = -0.9$.

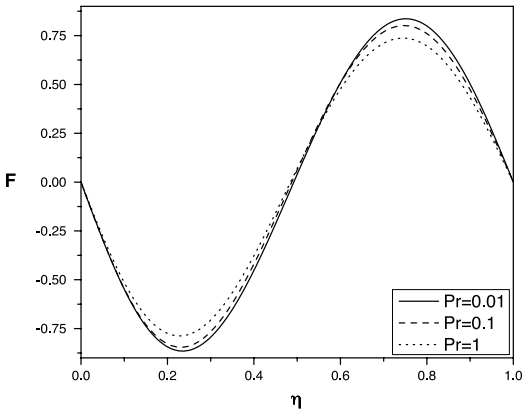

Fig. 27. Prandtl number Pr effect on F at $\gamma = -1$, $Re = 100$, $Pr = 0.01$, $\beta_i = 0.2$, $\beta_h = 0.20$, $Ha = 2.0$.

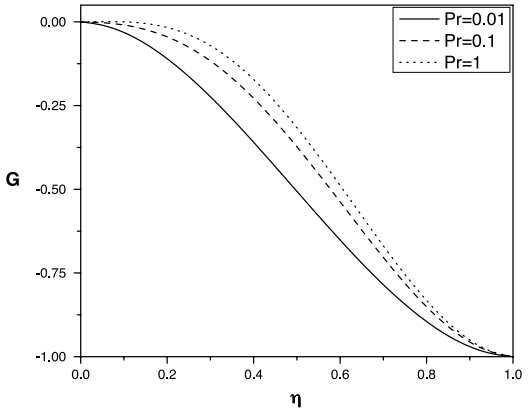

Fig. 28. Prandtl number Pr effect on G at $\gamma = -1$, $Re = 100$, $Pr = 0.01$, $\beta_i = 0.2$, $\beta_h = 0.20$, $Ha = 2.0$.

In order to pursue the convergence of the HAM solutions to the exact ones, the graphs for the ratio (following the recent work of [21])

$$\beta_H = \left|\frac{H_m(h)}{H_{m-1}(h)}\right|, \qquad \beta_G = \left|\frac{G_m(h)}{G_{m-1}(h)}\right|, \qquad \beta_\theta = \left|\frac{\theta_m(h)}{\theta_{m-1}(h)}\right| \tag{41}$$

against the number of terms m in the homotopy series is presented in Figs. 8–10. Figures strongly indicate that a finite limit of β will be attained in the limit of $m \to \infty$, which will remain less than unity (actually figures imply a limit of 0.12, 0.14, 0.096 for H, G and θ respectively). The velocity and temperature solutions seem to converge in an oscillatory manner requiring more terms in the homotopy series. Thus, the convergence to the exact solution is assured by the HAM method.

5. Results and discussion

The solutions for $F(\eta)$, $G(\eta)$, $H(\eta)$ and $\theta(\eta)$ have been computed and shown graphically in Figs. 11–30. The effects of magnetic parameter (Ha), Hall parameter (β_h), Ion-slip parameter (β_i), couple stress fluid parameter (α) and Prandtl Pr effect have been discussed. To study the effects of Ha, β_h, β_i, S and Pr, computations were carried out by taking $\gamma = -1$, $B = 0.05$.

Figs. 11–14 display the effect of the magnetic parameter Ha on $F(\eta)$, $G(\eta)$, $H(\eta)$ and $\theta(\eta)$. It can be observed that the velocities $F(\eta)$, $G(\eta)$ and $H(\eta)$ decreases with an increase in parameter Ha, while temperature distribution is independent of the magnetic field. This is because of the applied axial magnetic field, which gives rise to resistive force known as Lorentz force of an electrically conducting fluid in a rotating system.

The variation of velocity components $F(\eta)$, $G(\eta)$, $H(\eta)$ and temperature $\theta(\eta)$ with β_h is shown in Figs. 15–18. We see that the dimensionless velocity components $F(\eta)$, $H(\eta)$ decrease and $G(\eta)$ increases with an increase in parameter β_h. The inclusion of Hall parameter decreases the resistive force imposed by the magnetic field due to its effect in reducing the effective conductivity. As the energy equation is independent of Hall parameter, temperature have no significant change with the Hall parameter.

Figs. 19–22 represent the effect of the Ion-slip parameter β_i on $F(\eta)$, $G(\eta)$, $H(\eta)$ and $\theta(\eta)$. We see that from the velocities $F(\eta)$ and $G(\eta)$ decrease with an increase in parameter β_i. Fig. 21 depicts that the induced flow in the φ-direction increases

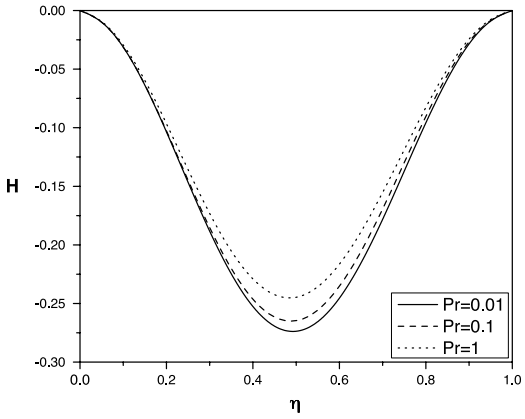

Fig. 29. Prandtl number Pr effect on H at $\gamma = -1$, $Re = 100$, $Pr = 0.01$, $\beta_i = 0.2$, $\beta_h = 0.20$, $Ha = 2.0$.

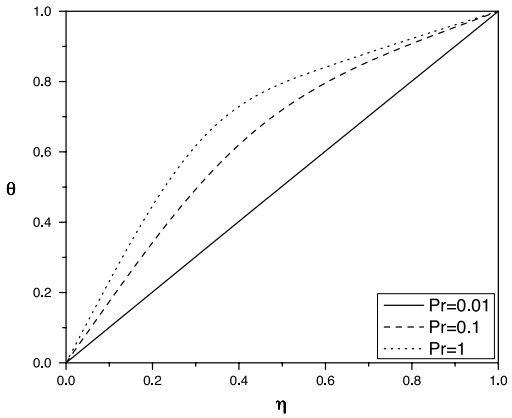

Fig. 30. Prandtl number Pr effect on θ at $\gamma = -1$, $Re = 100$, $Pr = 0.01$, $\beta_i = 0.2$, $\beta_h = 0.20$, $Ha = 2.0$.

with an increase in the parameter β_i. As β_i increases the effective conductivity also increases, in turn, decreases the damping force on the velocity component in the direction of the flow, and hence the velocity component in the flow direction increases. Unremarkable variation can be find in temperature distribution in Fig. 22, because of absence of Ion-slip parameter in energy equation.

Figs. 23–26 indicate the effect of the Couple stress fluid parameter S on $F(\eta)$, $G(\eta)$, $H(\eta)$ and $\theta(\eta)$. As the Couple stress fluid parameter S increases, the radial velocity $F(\eta)$, the tangential velocity $G(\eta)$ and axial velocity $H(\eta)$ decrease. It is also clear that the temperature $\theta(\eta)$ decreases with an increase in α. It can be noted that the velocity in case of couple stress fluid is less than that of a Newtonian fluid case. Thus, the presence of couple stresses in the fluid decreases the velocity and temperature.

In Figs. 27–30 with $B = 0.05$, the Prandtl number effect significantly alters the flow fields. For large Prandtl number, $Pr = 1$, the temperature function changes abruptly in the thin thermal boundary layer but remains uniform in large portion of the wheel space. As Pr decreases from 1 to 0.01, the thermal diffusion is getting more and more important and, then, the temperature variation appears notably in the whole domain rather than confined in a narrow region. For small Pr, the temperature gradient near the disk 1, i.e. $Z = 0$, is alleviated. Due to coupling of the Coriolis induced buoyancy in circumferential fluid motion and the Prandtl number effects, salient Pr-dependence of the circumferential velocity is presented.

6. Conclusions

In this paper, the Hall and Ion-slip effects on fully developed electrically conducting couple stress fluid flow between two parallel Disks has been studied. The governing equations are expressed in the non-dimensional form and are solved by using HAM. The features of flow characteristics are analyzed by plotting graphs and are discussed in detail. The main findings are summarized as follows:

- As the magnetic parameter increases, velocity decreases.
- The tangential velocity increased as the Hall and Ion-slip parameters increased.
- Increase in the Hall and Ion-slip parameters leads to decrease in radial and axial velocities.
- The presence of couple stresses in the fluid decreases the velocity and temperature.
- Increase in the Prandtl number leads to the increase in temperature and decrease in velocity.

Table 1
Optimal value of h_1 at different order of approximations.

Order	Optimal of h_1	Minimum of E_m
10	−1.015	2.93×10^{-7}
15	−1.03	1.36×10^{-8}
20	−1.03	-1.41×10^{-9}

Table 2
Optimal value of h_2 at different order of approximations.

Order	Optimal of h_2	Minimum of E_m
10	−1	-1.91×10^{-6}
15	−1	1.83×10^{-8}
20	−1	-5.59×10^{-10}

Table 3
Optimal value of h_3 at different order of approximations.

Order	Optimal of h_3	Minimum of E_m
10	−0.85	4.90×10^{-6}
15	−0.9	-2.75×10^{-8}
20	−0.9	-5.63×10^{-10}

Table 4
Convergence of HAM solutions for different order of approximations.

Order	$U(0)$	$W(0)$	$\theta(0)$
5	−0.0978237509	−0.5018297787	0.5436232327
10	−0.09782161851	−0.5018272424	0.5434752547
20	−0.09782161122	−0.5018272423	0.5434752142
30	−0.09782161122	−0.5018272423	0.5434752142
40	−0.09782161122	−0.5018272423	0.5434752142
50	−0.09782161122	−0.5018272423	0.5434752142

References

[1] T. von Karman, Laminar und turbulente reibung, Z. Angew. Math. Mech. 1 (1921) 233–244.
[2] C.Y. Soong, Theoretical analysis for axisymmetric mixed convection between rotating coaxial disks, Int. J. Heat Mass Transfer 39 (1996) 1569–1583.
[3] C.Y. Soong, Prandtl number effects on mixed convection between rotating coaxial disks, Int. J. Rotating Machinery 2 (1996) 161–166.
[4] M.F. Dimian, A.H. Essawy, Magnetic field effects on mixed convection between rotating coaxial disks, J. Engrg. Phys. Thermophys. 73 (5) (2000) 1082–1091.
[5] C.Y. Soong, Thermal buoyancy effects in rotating non-isothermal flows, Int. J. Rotating Machinery 7 (6) (2001) 435–446.
[6] C.Y. Soong, Flow structure and heat transfer between two disks rotating independently, J. Therm. Sci. 12 (2003) 62–76.
[7] L.M. Jiji, P. Ganatos, Microscale flow and heat transfer between rotating disks, Int. J. Heat Fluid Flow 31 (2010) 702–710.
[8] Atif Nazir, Tahir Mahmood, Analysis of flow and heat transfer of viscous fluid between contracting rotating disks, Appl. Math. Model. 35 (2011) 3154–3165.
[9] M. Batista, Steady flow of incompressible fluid between two co-rotating disks, Appl. Math. Model. 35 (2011) 5225–5233.
[10] F.N. Ibrahim, Unsteady flow between two rotating discs with heat transfer, J. Phys. D, Appl. Phys. 24 (1991) 1293–1299.
[11] E.A. Hamza, The magnetohydrodynamic effects on a fluid film squeezed between two rotating surfaces, J. Phys. D, Appl. Phys. 24 (1991) 547–554.
[12] M. Kumari, H.S. Takhar, G. Nath, Unsteady flow of a viscous fluid between two parallel disks with a time varying gap width and a magnetic field, Internat. J. Engrg. Sci. 33 (6) (1995) 781–791.
[13] H.A. Attia, Ion-slip effect on the flow due to a rotating disk, Arab. J. Sci. Eng. 29 (2A) (2004) 165–172.
[14] T. Hayat, M. Nawaz, Hall and ion-slip effects on three-dimensional flow of a second grade fluid, Internat. J. Numer. Methods Fluids 66 (2) (2011) 183–193.
[15] V.K. Stokes, Couple stresses in fluid, Phys. Fluids (1966) 1709–1715.
[16] V.K. Stokes, Theories of Fluids with Microstructure: An Introduction, Springer Verlag, New York, 1984.
[17] D. Srinivasacharya, K. Kaladhar, Mixed convection flow of couple stress fluid between parallel vertical plates with Hall and Ion-slip effects, Commun. Nonlinear Sci. Numer. Simul. 17 (2012) 2447–2462.
[18] D. Srinivasacharya, K. Kaladhar, Natural convection flow of a couple stress fluid between two vertical parallel plates with Hall and Ion-slip effects, Acta Mech. Sin. 28 (1) (2012) 41–50.
[19] S.J. Liao, Beyond Perturbation. Introduction to Homotopy Analysis Method, Chapman and Hall/CRC Press, Boca Raton, 2003.
[20] S.J. Liao, On the homotopy analysis method for nonlinear problems, Appl. Math. Comput. 147 (2) (2004) 499–513.
[21] M. Turkyilmazoglu, Numerical and analytical solutions for the flow and heat transfer near the equator of an MHD boundary layer over a porous rotating sphere, Int. J. Therm. Sci. 50 (2011) 831–842.
[22] S.J. Liao, An optimal homotopy-analysis approach for strongly nonlinear differential equations, Commun. Nonlinear Sci. Numer. Simul. 15 (2010) 2003–2016.